Immobilization and Aggregation of the Antimicrobial Peptide Protegrin-1 in Lipid Bilayers Investigated by Solid-State NMR†

Jarrod J. Buffy,‡ Alan J. Waring,§ Robert I. Lehrer,§ and Mei Hong*,‡

Department of Chemistry, Iowa State University, Ames, Iowa 50011, and Department of Medicine, University of California at Los Angeles School of Medicine, Los Angeles, California 90095

Received July 8, 2003; Revised Manuscript Received September 18, 2003

ABSTRACT: The dynamics and aggregation of a β-sheet antimicrobial peptide, protegrin-1 (PG-1), are investigated using solid-state NMR spectroscopy. Chemical shift anisotropies of F12 and V16 carbonyl carbons are uniaxially averaged in 1,2-dilauryl-*sn*-glycero-3-phosphatidylcholine (DLPC) bilayers but approach rigid-limit values in the thicker 1-palmitoyl-2-oleoyl-*sn*-glycerol-3-phosphatidylcholine (POPC) bilayers. The Cα−Hα dipolar coupling of L5 is scaled by a factor of 0.16 in DLPC bilayers but has a near-unity order parameter of 0.96 in POPC bilayers. The larger couplings of PG-1 in POPC bilayers indicate immobilization of the peptide, suggesting that PG-1 forms oligomeric aggregates at the biologically relevant bilayer thickness. Exchange NMR experiments on F12 ^{13}CO-labeled PG-1 show that the peptide undergoes slow reorientation with a correlation time of 0.7 ± 0.2 s in POPC bilayers. This long correlation time suggests that in addition to aggregation, geometric constraints in the membrane may also contribute to PG-1 immobilization. The PG-1 aggregates contact both the surface and the hydrophobic center of the POPC bilayer, as determined by ^{1}H spin-diffusion measurements. Thus, solid-state NMR provides a wide range of information about the molecular details of membrane peptide immobilization and aggregation in lipid bilayers.

Antimicrobial peptides form in many organisms part of the innate immune system against bacterial, fungal, and viral attacks (*1*). They kill invading microbes by destroying their cell membranes. Aggregation or oligomerization of these peptides is often suspected to be important in disrupting the membranes of the target cells. This is manifested in various structural models for antimicrobial activity. For instance, the barrel-stave model postulates that transmembrane peptides form helical bundles (*2*, *3*) to deplete the membrane potential. The carpet model hypothesizes that at sufficiently high concentrations, the peptides micellize the bilayer, thereby destroying the membrane (*4*). However, direct evidence of antimicrobial peptide aggregation in the membrane is scarce. In general, fluorescence resonance energy transfer and fluorescence spectroscopy can be used to detect peptide aggregation through quenching of the fluorophore or concentration-dependent fluorescence emission intensities (*5*). While these methods have been used to study the formation of oligomeric helical bundles, amyloid fibrils (*6*−*8*), and peptide association in micelles and bilayers (*9*−*11*), they require bulky extrinsic probes, which can cause non-negligible structural perturbations to the peptides of interest.

Solid-state NMR provides a nonperturbing tool for obtaining detailed information about peptide aggregation. Because of the lack of a requirement on isotropic mobility and long-range order, solid-state NMR is ideally suited to the study of insoluble and amorphous peptides. The extent of peptide aggregation may be determined in two ways. The first involves the measurement of intermolecular distances through nuclear spin dipole−dipole couplings. This approach has been used, for example, to identify interhelical contacts in glycophorin A (*13*) and the intermolecular association of amyloid fibrils (*12*). Alternatively, one can probe peptide aggregation through molecular motion. It has been shown that small membrane peptides with fewer than 20 amino acids usually undergo uniaxial motion around the bilayer normal on time scales shorter than 10^{-5} s. This was observed in gramicidin A (*14*), gramicidin S (*15*), ovispirin (*16*), and the transmembrane fragment of the M2 peptide proton channel (*17*). The propensity for rigid-body rotation can be readily understood in the context of the hydrodynamic model (*18*), as small-molecule additives to the two-dimensional liquid-crystalline bilayer experience the same motional driving force as the lipids. Once the peptides aggregate, however, their mobility decreases. Thus, molecular motion can serve as an indicator of the oligomerization of membrane peptides.

Protegrin-1 (PG-1, molecular mass of 2154 Da) is an 18-residue broad-spectrum antimicrobial peptide found in porcine leukocytes (*19*). It kills Gram-positive bacteria, Gram-negative bacteria, and fungi (*20*) and has modest antiviral activities against HIV-1 (*21*). PG-1 forms an antiparallel β-strand in solution (*22*, *23*), where the two

† M.H. gratefully acknowledges the Beckman Foundation and the Alfred P. Sloan Foundation (Grant BR-4151) for a research fellowship. This work is supported by National Institutes of Health Grants GM-066976 to M.H. and Grants AI-22839 and AI-37945 to A.J.W. and R.I.L.

* To whom correspondence should be addressed: Department of Chemistry, Iowa State University, Ames, Iowa 50011. Telephone: (515) 294-3521. Fax: (515) 294-0105. E-mail: mhong@iastate.edu.

‡ Iowa State University.

§ University of California at Los Angeles School of Medicine.

10.1021/bi035187w CCC: $25.00
Published on Web 11/01/2003

strands are stabilized by two disulfide bonds among the four Cys residues. This disulfide-stabilized β-hairpin motif is common to a number of other antimicrobial peptides such as human defensins and tachyplesin (*1*).

Evidence of PG-1 aggregation in lipid bilayers is so far sparse in the literature. In aqueous and dimethyl sulfoxide solutions, PG-1 is monomeric (*22*, *23*). In DPC micelles, ^{1}H NOE data suggested dimer formation (*24*). Neutron diffraction patterns of fully hydrated DMPC membranes containing 1:30 (*P*:*L*) PG-1 suggest that the peptide aggregates to form stable pores (*25*). Lowering the temperature or hydration level of the bilayers resulted in crystallization of these pores, implying cooperative action of several PG-1 molecules in disrupting the bilayer.

In this work, we use magic-angle spinning (MAS) solid-state NMR techniques to investigate the dynamic structure and aggregation of PG-1 in phosphocholine bilayers whose chain lengths range from 12 to 18 carbons. The lipid chain length dependence of PG-1 action was seen in our recent orientation study using uniaxially aligned membranes (*26*). We found that the 12-carbon 1,2-dilauryl-*sn*-glycero-3-phosphatidylcholine (DLPC) bilayers maintain their orientational order upon PG-1 binding, while the 16- and 18-carbon 1-palmitoyl-2-oleoyl-*sn*-glycerol-3-phosphatidylcholine (POPC) bilayers become completely disordered at peptide concentrations of greater than 3%. In DLPC bilayers, the β-strand axis is tilted by 55° from the bilayer normal (*26*) and is completely inserted (*27*). However, little is known about PG-1 orientation, insertion, and dynamics at the biologically relevant thickness of POPC bilayers. In this study, we use MAS NMR to circumvent the need for uniaxially aligned samples and to probe PG-1 mobility from which we derive information about its aggregation. We show that at room temperature, and at a peptide:lipid molar ratio (*P*:*L*) of 1:20, PG-1 is largely immobilized in POPC bilayers but undergoes fast uniaxial motion around the membrane normal in DLPC bilayers. This is manifested in both ^{13}C chemical shift anisotropies and ^{13}C$-^1$H dipolar couplings of isotropically labeled peptides. Using exchange NMR, we found that the slowest reorientational motion of PG-1 in POPC membranes has a correlation time of 0.7 s. This slow rate suggests that, in addition to aggregation, geometric constraints and electrostatic attractions also contribute to PG-1 immobilization. Finally, ^{1}H spin-diffusion experiments indicate that the PG-1 aggregates contact both the membrane surface and the hydrophobic center of the bilayer.

EXPERIMENTAL PROCEDURES

Materials. 1,2-Dilauryl-*sn*-glycero-3-phosphatidylcholine (DLPC), 1,2-dimyristoyl-*sn*-glycero-3-phosphatidylcholine (DMPC), and 1-palmitoyl-2-oleoyl-*sn*-glycerol-3-phosphatidylcholine (POPC) were purchased from Avanti Polar Lipids (Alabaster, AL) and used without further purification. The acyl chain lengths are 12:0 for DLPC, 14:0 for DMPC, and 16:0 and 18:1 for POPC. The main phase transition temperatures are -1 °C for DLPC, 23 °C for DMPC, and -2 °C for POPC. Trifluoroethanol (TFE) and chloroform were purchased from Aldrich Chemicals (Milwaukee, WI). Citric acid and sodium hydroxide were purchased from Fischer Scientific. Isotopically labeled amino acids, including Val ^{13}CO, Phe ^{13}CO, and Leu ^{13}Cα, were obtained from Cambridge Isotope Laboratories (Andover, MA) and were converted to their Fmoc derivatives by AnaSpec, Inc. (San Jose, CA). PG-1 (NH_2-RGGRLCYCRRRFCVCVGR-$CONH_2$) was synthesized according to previously published procedures (*26*). The labeled amino acids were incorporated at L5, F12, and V16 (Figure 1).

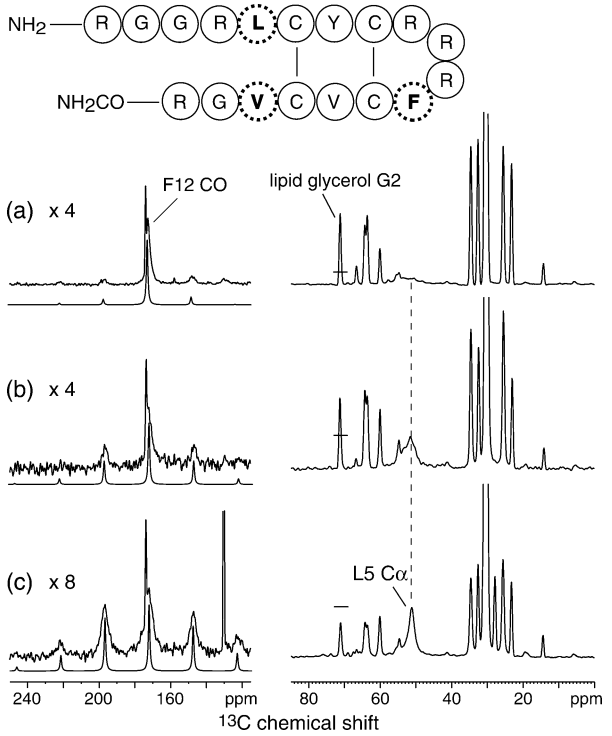

FIGURE 1: ^{13}C CP-MAS spectra of F12 ^{13}CO- and L5 ^{13}Cα-labeled PG-1 in (a) DLPC ($T = 295$ K), (b) DMPC ($T = 313$ K), and (c) POPC ($T = 295$ K) bilayers with 2.5 kHz spinning. Note the increased carbonyl sideband intensities and higher L5 Cα signal with increasing lipid chain length. For clarity, the carbonyl intensities are scaled up relative to the aliphatic signals, and the L5 Cα intensity is shown as a horizontal bar. Best fits for the carbonyl spinning sideband patterns are shown below each experimental spectrum. The number of scans (NS) ranges from 8000 to 22 000.

Sample Preparation. Unoriented membrane mixtures were prepared by codissolving ~5 mg of PG-1 and 30 mg of lipids in TFE and chloroform solutions to achieve a *P*:*L* of 1:20. The combined solution was dried under a stream of nitrogen gas and the resulting membrane film redissolved in a small amount of cyclohexane and lyophilized. For most samples, which were prepared previously for measuring the depth of insertion (*27*), the mixture was resuspended in a citrate buffer [10 mM citrate and 10 mM KCl (pH 4.8)] and extruded across polycarbonate membrane filters (Avanti Polar Lipids) with a pore size of 1 μm to obtain relatively uniform vesicles. The solution was then centrifuged at 150000*g* for 2 h, pelleted, lyophilized, and rehydrated to 35% (w/w) water to obtain fully hydrated membrane mixtures. Since the experiments described here do not require uniform vesicles, the DMPC/PG-1 sample produced just for the current study bypassed the extrusion and ultracentrifugation steps, and was directly hydrated to 35% in the NMR rotor.

Solid-State NMR. NMR experiments were carried out on a Bruker (Karlsruhe, Germany) DSX-400 spectrometer

operating at a resonance frequency of 400.49 MHz for ^{1}H and 100.70 MHz for ^{13}C (9.4 T). The samples were packed into 4 mm zirconia rotors and placed in the spinning module of an MAS probe. Low-temperature experiments (243 K) were performed using air cooled through a heat exchanger immersed in liquid nitrogen. The temperature was maintained within 2 K of the desired value. Typical radio frequency pulse lengths were 5 μs for ^{13}C and 3.5−4.0 μs for ^{1}H. Short cross-polarization (CP) contact times of 0.3−0.5 ms were used to minimize lipid background signals. Sample spinning speeds were regulated to within 3 Hz using a Bruker pneumatic control unit. Typical recycle delays were 2 s, and acquisition times were 30 ms. ^{13}C chemical shifts were referenced externally to the β-glycine carbonyl signal at 176.4 ppm, and ^{1}H chemical shifts were referenced to the ω-CH_3 signal of lipids at 0.9 ppm.

Spinning Sideband Analysis. MAS spinning sideband spectra were analyzed using the program HBA (http://casgm3.anorg.chemie.uni-tuebingen.de/klaus/index.html) to extract chemical shift principal values. The program is based on an extended Herzfeld−Berger analysis (*28*), allowing input of up to 15 spinning sideband intensities and values of μ (span) in the range of 0−30. The tensor parameters were refined by nonlinear least-squares fitting. The resulting chemical shift tensor was input into the SIMPSON program (*29*) (http://nmr.imsb.au.dk/bionmr/software /simpson.php) to simulate the experimental spectra. We report the chemical shift anisotropy (CSA) using the anisotropy parameter δ ($=\delta_{zz} - \delta_{iso}$) and the asymmetry parameter η [$= |\delta_{yy} - \delta_{xx}|/\delta$, where δ_{zz} is the principal value furthest from the isotropic shift and δ_{yy} is the principal value closest to the isotropic shift (*30*)].

Two-Dimensional (2D) ^{13}C−^{1}H Dipolar Coupling Measurement. The Cα−Hα dipolar coupling of L5 was measured using a 2D Lee−Goldburg cross-polarization (LG-CP) experiment (*31*, *32*). During the CP contact time, ^{1}H magnetization is spin-locked along an effective field tilted by the magic angle (54.7°) from the external magnetic field. This suppresses the homonuclear ^{1}H−^{1}H dipolar couplings while retaining a scaled ^{13}C−^{1}H dipolar coupling. The CP contact time is incremented to form the evolution period (t_1) of the 2D experiment. ^{13}C detection during the t_2 period resolves the C−H couplings according to the ^{13}C isotropic chemical shift of the individual sites. The experiment was carried out at a spinning speed of 10 kHz.

^{13}C Exchange Experiment. Slow reorientation of PG-1 on the time scale of 10 ms or longer was probed using the centerband-only detection of exchange (CODEX) technique (*33*). The ^{13}C magnetization evolves under the anisotropic chemical shift interaction, which is recoupled by rotor-synchronized 180° pulses (*34*). The magnetization is stored along the *z*-axis for a mixing period, τ_m, followed by an identical train of rotor-synchronized 180° pulses. If no reorientation occurs during τ_m, the chemical shift evolution is completely refocused by the two pulse trains and yields a full stimulated echo. Reorientation during τ_m changes the anisotropic frequency and prevents the complete refocusing of the chemical shift interaction, thus decreasing the echo intensity. The decay of the echo intensity as a function of the exchange mixing time yields the correlation time of motion. To correct for spin−lattice (T_1) relaxation effects during τ_m, the dephased spectrum (S) is normalized to a reference spectrum (S_0) acquired with a short τ_m and a long *z*-filter such that the total duration of the *z*-magnetization is the same as in the dephasing experiment. The normalized intensity S/S_0 represents pure orientational exchange. Mixing times of 5 ms to 3.5 s and a spinning speed of 6 kHz were used in these experiments.

^{1}H Spin-Diffusion Experiment. A 2D ^{1}H spin-diffusion experiment was used (*35*) to investigate the location of PG-1 in the POPC bilayer. The experiment selects the ^{1}H magnetization of the mobile lipid groups and water, whose depths along the bilayer normal are well-known, and monitors its transfer to the protons of the rigid peptide. The chemical shifts of the mobile protons were encoded in the indirect dimension of the 2D spectra, while the ^{13}C chemical shifts of the peptide were detected in the direct dimension. The 2D peak intensities as a function of the spin-diffusion mixing time yield a magnetization transfer curve that reflects the proximity of the lipid protons to the peptide protons. The experiment requires the peptide to be more rigid than the lipids; thus, it is ideally suited to the POPC/PG-1 mixture in which the peptide is mostly immobilized (see Results). Since the peptide is much more rigid than the lipids, magnetization transfer within the peptide is much faster than through the lipid matrix or across the interface from the lipid to the peptide. As a result, this room-temperature spin-diffusion experiment reveals only the global topology of the peptide in the membrane, but does not give precise site-resolved distances.

Spin-diffusion buildup curves were simulated using a one-dimensional lattice model (*35*, *36*) in which each ^{1}H spin passes a fraction of its magnetization to its two neighbors and in turn receives magnetization according to the discrete diffusion equation:

$$\frac{\Delta M_i}{\Delta t} = -2\Omega M_i + \Omega M_{i+1} + \Omega M_{i-1} \qquad (1)$$

The rate of magnetization transfer Ω ($\Omega = D/a^2$) is related to the lattice spacing a and the diffusion coefficient D. We used a lattice spacing of 2 Å in all simulations. The transfer rate can be estimated from experimentally measured couplings or order parameters; thus, the diffusion coefficient D can be derived. For the chain end ω and headgroup Hγ, ^{2}H NMR indicates an order parameter of ∼0.05 (*16*). This corresponds to a coupling of ∼400 Hz between two vicinal protons separated by 2.4 Å, and thus a diffusion coefficient of 0.015 nm^2/ms. The peptide has an average order parameter of ∼0.72 based on the chemical shift anisotropies of carbonyl carbons in POPC (see Results). This gives a dipolar coupling of ∼6 kHz between vicinal protons, and a diffusion coefficient of 0.25 nm^2/ms (*37*). For interfacial magnetization transfer from the lipid to the peptide, the diffusion coefficient is usually much smaller due to the fast uniaxial rotation and lateral diffusion of lipids. Since it cannot be measured readily, the interfacial diffusion coefficient (D_{int}) was treated as an adjustable parameter in the simulations. Other input parameters for the simulations include the thickness of the interface, which is 2 Å, and the thickness of the source protons, which is 2−4 Å for Hγ and ω-CH_3. The length of the peptide was taken to be 30 Å based on the solution structure (*23*).

Table 1: PG-1 F12 and V16 Carbonyl Chemical Shift Anisotropies in Various Phosphocholine Lipids

^{13}CO	T (K)	lipid	$\delta_{11}{}^a$ (ppm)	$\delta_{22}{}^a$ (ppm)	$\delta_{33}{}^a$ (ppm)	δ_{iso} (ppm)	δ^b (ppm)	η^b
F12	295	DLPC	202	159	156	172.3	30	0.12
	313	DMPC	219	172	126	172.3	47	0.98
	295	POPC	231	176	109	172.0	−63	0.87
V16	295	DLPC	216	152	148	172.0	44	0.09
	295	POPC	220	177	117	171.6	−55	0.79
V16	243	DLPC	242	181	96	172.8	−77	0.80
	243	POPC	243	184	91	172.8	−82	0.72

[a] The principal values δ_{11}, δ_{22}, and δ_{33} are assigned in the order of decreasing chemical shifts. [b] The anisotropy parameter δ and the asymmetry parameter η are defined using the δ_{xx}, δ_{yy}, and δ_{zz} convention (*30*), where δ_{zz} is the principal value furthest from the isotropic shift while δ_{yy} is the principal value closest to the isotropic shift.

RESULTS

Carbonyl Chemical Shift Anisotropies of PG-1 in Different Chain Length Lipids. The rigid-limit amide carbonyl chemical shift tensor typically has an anisotropy δ of 80 ± 5 ppm and an asymmetry parameter η of 1 (*38*). Reduction of δ and a change in η signify molecular motion. Figure 1 shows the ^{13}C CP-MAS spectra of F12 ^{13}CO-labeled PG-1 in three lipids with different chain lengths: 12:0 DLPC, 14:0 DMPC, and 16:0 and 18:1 POPC. The spectra were acquired at a slow spinning speed of 2.5 kHz to generate a large number of sidebands to obtain precise chemical shift principal values. The spectra of the DLPC- and POPC-bound PG-1 were measured at 295 K, which is 23 K higher than the main phase transition temperatures of the lipids. The DMPC/PG-1 spectrum was acquired at 313 K, 17 K higher than the phase transition temperature. It can be seen that the sideband intensities are the weakest in the thinnest bilayer, DLPC, and increase with the chain length. This means that the ^{13}CO chemical shift tensor is motionally averaged in DLPC bilayers but becomes more rigid in thicker lipid bilayers. A Herzfeld−Berger analysis yielded an anisotropy of 30 ppm in DLPC, 47 ppm in DMPC, and −63 ppm in POPC (Table 1). In addition to δ, the asymmetry parameter of the chemical shift tensor also differs significantly. In DLPC bilayers, the F12 ^{13}CO tensor has a nearly vanishing η of 0.12, indicating that PG-1 rotates uniaxially around the bilayer normal. In contrast, in DMPC and POPC bilayers, η approaches 1 (Table 1), similar to that of a rigid ^{13}CO tensor.

The chain length dependence of the F12 carbonyl CSA is confirmed by the V16 carbonyl spectra. Figure 2c shows the static CP spectrum of V16 ^{13}CO in DLPC bilayers. The lipid background intensities were removed by subtracting a direct polarization (DP) spectrum (Figure 2b) of the mixture from the CP spectrum (Figure 2a). The DP spectrum preferentially enhances the signals of the mobile lipids, while the CP spectrum enhances the signals of the rigid peptide with stronger C−H dipolar couplings. The lipid-free V16 ^{13}CO pattern shows an axially symmetric line shape with an η of 0.09, a δ of 44 ppm, and a distinct 90° orientation peak at 150 ppm. The small η and the reduction of the anisotropy from the rigid-lattice value are both consistent with the uniaxial symmetry of the liquid-crystalline bilayers. Since F12 and V16 are located at opposite ends of the β-hairpin but exhibit similar asymmetry parameters of nearly zero, the uniaxial motion must be rigid-body rather than segmental. In contrast, the MAS spectrum (Figure 2d) of V16 ^{13}CO in POPC lipids shows a larger δ of −55 ppm and an η of 0.79, similar to the F12 ^{13}CO CSA tensor parameters in POPC.

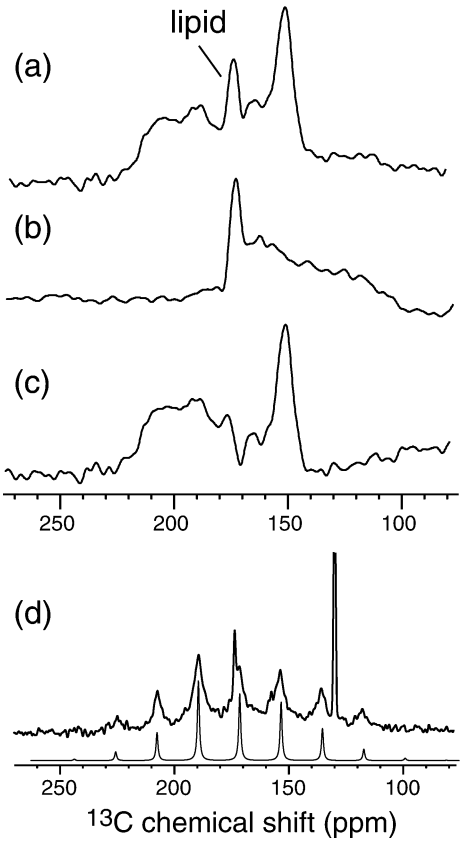

FIGURE 2: ^{13}C spectra of V16 ^{13}CO labeled PG-1 at 295 K. (a−c) Static spectra of PG-1 in DLPC bilayers. (a) CP spectrum, including contributions from both the lipid and the peptide. (b) DP spectrum, showing mostly the lipid carbonyl intensity. (c) Difference spectrum of spectrum a minus spectrum b, giving the signals of only V16 ^{13}CO. (d) CP-MAS spectrum of V16 ^{13}CO-labeled PG-1 in POPC lipids. The spinning speed was 1.8 kHz. The best-fit simulation is obtained with a δ of −55 ppm and an η of 0.79. The 130 ppm signal results from the lipid C═C site of POPC. NS = 15000−30000.

The carbonyl CSA is useful not only as a motional probe but also as a semiquantitative indicator of hydrogen bonding. Quantum chemical calculations (*39*) and solid-state NMR experiments (*40*, *41*) have shown that the carbonyl chemical shift tensor is largely independent of the backbone (ϕ and ψ) torsion angles but is sensitive to the C═O to H−N hydrogen bond distance. The middle principal value, δ_{22}, whose axis is aligned with the C═O bond, is shifted downfield in shorter hydrogen bonds. For example, in Ala-containing model peptides, δ_{22} was found experimentally to be 175 ppm for N−O distances of ≥3 Å but increases to 195 ppm for an N−O distance of 2.75 Å (*40*).

To assess the degree of hydrogen bonding of PG-1 in POPC versus DLPC lipids, we measured the ^{13}C CP-MAS spectra at 243 K, well below the phase transition temperatures of the two lipids. The low temperature eliminates motional averaging so that the spectra reflect only static structural features. Although not directly involved in intermolecular hydrogen bonding, the V16 carbonyl should be sensitive to structural changes that result from peptide aggregation. Figure 3 shows the V16 carbonyl sideband

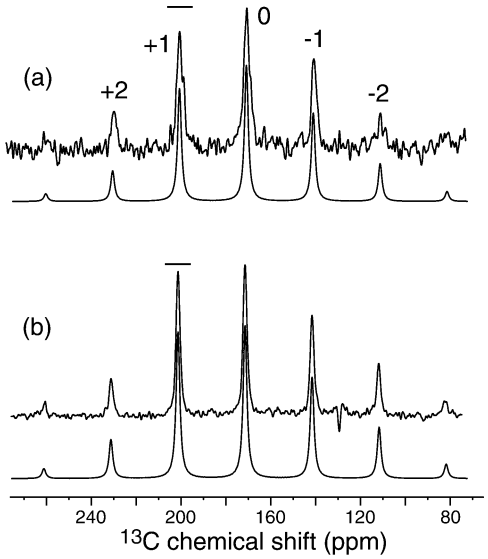

FIGURE 3: ^{13}C CP-MAS spectrum of V16 ^{13}CO-labeled PG-1 at 243 K in (a) DLPC lipids and (b) POPC lipids. The spinning speed was 3 kHz. The lipid background signals, measured at the same temperature, were subtracted. Note the higher intensity of the +1 sideband in POPC than in DLPC lipids. Horizontal bars denote the intensity of the center band. NS = 3000−13000.

spectra in DLPC (top) and POPC (bottom) lipids. The lipid background intensities were removed by subtracting the spectra of pure DLPC and POPC samples. It can be seen that the first-order sideband downfield from the center band is noticeably higher in the POPC-bound PG-1 than in the DLPC-bound PG-1. This indicates that δ_{22} is shifted downfield in POPC bilayers compared to DLPC bilayers. Herzfeld−Berger analysis and best-fit simulation yielded a δ_{22} of 184 ppm for the POPC-bound PG-1 and 181 ppm for the DLPC-bound PG-1. These translate to η values of 0.72 for POPC and 0.80 for DLPC (Table 1). The smaller η in POPC bilayers suggests a shorter C═O to H−N hydrogen bond at the V16 site.

Cα−Hα Dipolar Couplings of L5 in Lipids with Different Chain Lengths. Further evidence of the lipid-regulated PG-1 mobility is obtained from the Cα−Hα dipolar coupling of L5. Dipolar couplings depend both on the internuclear distance and on molecular motion. For a fixed internuclear distance, reduction of the coupling strength from its rigid-lattice value can only result from motional averaging. The scaling factor between the measured coupling $\bar{\delta}_{CH}$ and the rigid-limit value δ_{CH} is the bond order parameter S_{CH} ($=\bar{\delta}_{CH}/\delta_{CH}$), which provides information about the amplitude of motion and, in favorable cases, the orientation of the C−H bond relative to the motional axis.

We measured the L5 Cα−Hα dipolar coupling using the 2D LG-CP experiment (*32*). The dipolar spectrum is obtained after baseline correction, inversion, and Fourier transformation of the t_1 signal. Figure 4a displays part of the 2D spectrum of the POPC/PG-1 sample, where the L5 Cα isotropic shift is detected at 52 ppm. Its dipolar cross section (Figure 4b) shows a splitting of 11.9 kHz. After correcting for the Lee−Goldburg scaling factor of 0.577, we obtain an unscaled dipolar coupling of 20.6 kHz. The rigid-limit one-bond C−H dipolar coupling is 22.7 kHz. Bond vibration scales down the dipolar coupling by ∼5%, as measured on small model compounds with no segmental motions (*32*). Thus, the L5 Cα−Hα order parameter is 20.6/(22.7 × 0.95) = 0.96. The near-unity order parameter indicates that the Leu Cα segment is mostly immobilized. If we assume that the residual segmental motion of the C−H bond is axially symmetric, then S_{CH} is related to the root-mean-square (rms) amplitude of motion by the relationship $S_{CH} = 1 - {}^3/_2\langle\theta^2\rangle$. This yields a small rms angle of 10°.

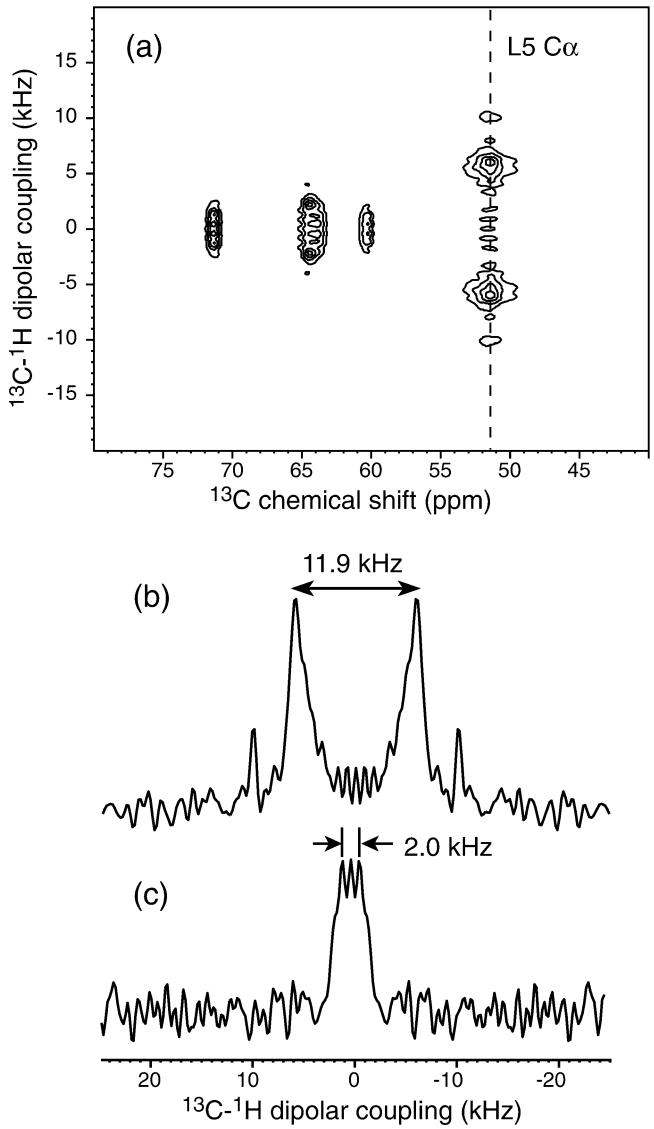

FIGURE 4: L5 Cα−Hα dipolar coupling of PG-1 at 295 K. (a) 2D LG-CP spectrum of PG-1 in POPC lipids. L5 Cα resonates at 52 ppm. (b) L5 dipolar cross section from spectrum a, showing a splitting of 11.9 kHz. (c) L5 dipolar cross section of the DLPC/PG-1 mixture, showing a splitting of 2 ± 1 kHz. In the 2D experiments, 832 scans (b) and 1312 scans (c) were co-added for each t_1 slice.

In contrast, the DLPC-bound PG-1 shows a much weaker Cα−Hα dipolar coupling of ∼2 ± 1 kHz (fwhm of 3.5 kHz) (Figure 4c), corresponding to an order parameter S_{CH} of 0.16 ± 0.08. Thus, PG-1 undergoes large-amplitude motion in DLPC bilayers. More detailed information about the angle of motion can be obtained by the following arguments. First, the two carbonyl CSAs measured here and the V16 ^{15}N CSA determined previously (*26*) indicate unambiguously that PG-1 rotates uniaxially in DLPC bilayers. Second, the previous orientation determination of PG-1 in DLPC lipids found that the β-sheet plane of the peptide adopts a well-defined orientation of 48° with respect to the bilayer normal. This

means that the peptide does not undergo uniaxial rotation around its own molecular axis. Third, the previous study also showed that the molecular order parameter, which describes the wobbling of the molecular axis relative to the bilayer normal, equals nearly 1. In other words, the strand axis maintains a constant orientation with the bilayer normal. Finally, it is reasonable to assume that there is little internal segmental motion at the backbone Cα segment. Under these conditions, the only motion present in the DLPC-bound PG-1 is the rigid-body uniaxial rotation around the bilayer normal, i.e., diffusion on a cone. Then, S_{CH} is simply equated to $(3\cos^2\theta_{CH} - 1)/2$, where θ_{CH} is the angle between the L5 C−H bond and the bilayer normal. For an $|S_{CH}|$ of 0.16 ± 0.08, we find four degenerate solutions of $\cos\theta_{CH}$. One of these solutions, $\cos\theta_{CH} = -0.47 \pm 0.05$, gives a θ_{CH} of $118 \pm 4°$. This agrees well with the angle of 110° determined from oriented sample measurements (*26*).

The different mobility of PG-1 in DLPC and POPC bilayers is also manifested in the L5 Cα peak intensity in the ^{13}C CP-MAS spectra (Figure 1). The relative intensity of L5 Cα to the lipid signals increases substantially from DLPC to POPC. For example, the intensity ratio of L5 Cα to the lipid glycerol G2 is 1:10 in DLPC, 1:2 in DMPC, and 1:0.6 in POPC. The reduced intensity of L5 Cα in DLPC membranes indicates inefficient cross polarization due to large-amplitude motions, while the high intensity of the POPC-bound peptide indicates strong C−H dipolar couplings due to immobilization.

Slow Motions of PG-1 in POPC Lipids. While POPC-bound PG-1 is mostly immobilized on time scales shorter than the inverse of the chemical shift and dipolar interactions, it may undergo reorientational motions that are slow compared to these interactions. To investigate this, we applied the CODEX experiment (*33*, *42*), which detects slow molecular motions through the reduction in the stimulated echoes. The experiment was carried out on F12 ^{13}CO and L5 ^{13}Cα labeled PG-1 at a *P*:*L* of 1:20. Four rotor periods of 180° pulses were used to recouple the ^{13}CO CSA under a spinning speed of 6 kHz. This gives a total CSA recoupling time of 0.67 ms. Since the F12 ^{13}CO CSA is −63 ppm (Table 1), the dimension-less parameter $(2\pi\delta)Nt_r$ that determines the sensitivity of the experiment to small-amplitude motions equals 8.4π. This value is sufficiently large to detect small-angle motions (*33*).

Figure 5 displays a pair of representative CODEX dephased (*S*) and reference (S_0) spectra acquired with a mixing time of 0.7 s. At this long time, most lipid ^{13}C signals have dephased due to the short ^{13}C T_1 relaxation times. However, both the F12 ^{13}CO and L5 Cα signals survive well. The normalized pure exchange signal (S/S_0) of F12 ^{13}CO is 0.7. Plotting S/S_0 as a function of the mixing times (Figure 5c), we find a single-exponential decay with a correlation time of 0.7 ± 0.2 s to a constant plateau of 0.5.

PG-1 Topology in POPC Lipids. To obtain information about the location of PG-1 aggregates in the POPC bilayer, we carried out a ^{1}H spin-diffusion experiment, in which ^{1}H magnetization is transferred from mobile lipids to the rigid peptide via distance-dependent ^{1}H−^{1}H dipolar couplings. The magnetization of the mobile protons is selected by a T_2 filter and acts as the source of spin diffusion, while the PG-1 ^{13}C signals are detected to probe lipid-to-peptide transfer. The growth of the intensities as a function of the mixing time

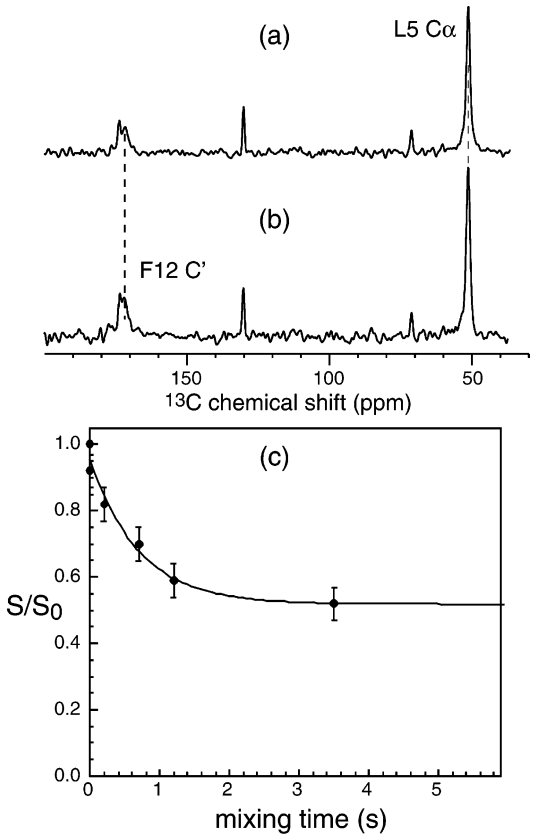

FIGURE 5: ^{13}C CODEX (a) dephased and (b) reference spectra of F12 ^{13}CO- and L5 ^{13}Cα-labeled PG-1 in POPC lipids with a mixing time of 0.7 s. The lipid intensities have mostly been dephased due to the short T_1 relaxation times. NS = 4000 (a) and 2000 (b). (c) Normalized dephasing S/S_0 of F12 ^{13}CO as a function of the mixing time.

provides information about the separation of the peptide from the various lipid segments. In liquid-crystalline bilayers, the spectrally resolved mobile protons include the chain-end ω-CH_3 at the center of the bilayer, the CH_2 groups in the middle of the acyl chains, the headgroup trimethylamine protons Hγ, and the water protons between opposing bilayers.

Figure 6a shows a representative 2D ^{1}H spin-diffusion spectrum acquired with a mixing time of 200 ms. The L5 ^{13}Cα peak at 52 ppm exhibits cross-peaks with all four mobile protons. The ^{1}H cross sections at several mixing times are shown in Figure 6b to illustrate the growth of the peak intensities. After integrating the 2D peak intensities and correcting for ^{1}H T_1 relaxation times, we obtained the spin-diffusion buildup curves for ω-CH_3, CH_2, and Hγ (Figure 7). The water spin-diffusion curve is not analyzed because of its short ^{1}H T_1 relaxation time. The first thing to notice is that none of the three curves reached a plateau even at the longest mixing time that was used, 529 ms. The CH_2 and Hγ signals continue to rise, while the ω-CH_3 signal is too weak at 529 ms to permit a precise measurement of its intensity. Longer mixing time spectra were difficult to obtain due to the short ^{1}H T_1 relaxation times and the resulting poor sensitivity. Second, all three experimental curves display non-negligible intensities at short mixing times, but the intensities increase only slowly with time. This is best illustrated by comparing them with the calculated buildup curves for a distance of 4 Å (top dashed line) and 16 Å (bottom dashed line) between the lipid and the peptide (Figure 7a). The 4 Å buildup curve matches the initial experimental intensities of

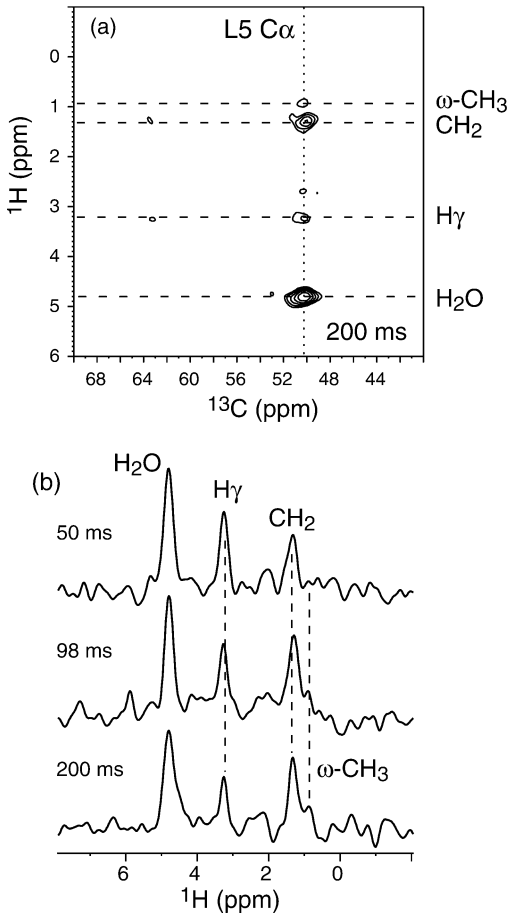

FIGURE 6: (a) 2D $^1H-^{13}C$ correlation spectrum of the PG-1/POPC mixture at a spin-diffusion mixing time of 200 ms. (b) ^1H cross sections at the L5 Cα chemical shift for several spin-diffusion mixing times. Typically, 384 scans were acquired for each t_1 slice of the 2D experiment.

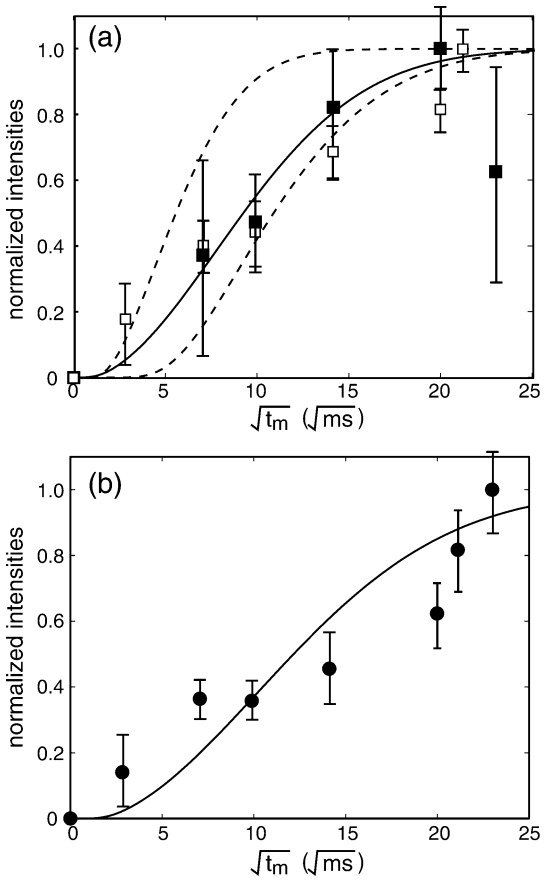

FIGURE 7: ^1H spin-diffusion buildup curves from lipid protons to PG-1. (a) ω-CH_3 (■) and CH_2 (□). Dashed lines correspond to calculated spin-diffusion curves for a lipid−peptide separation of 4 Å (top) or 16 Å (bottom). A D_{int} of 0.0025 nm^2/ms was used. The solid line is the calculated curve for a 2 Å separation with a D_{int} of 0.0005 nm^2/ms. (b) Headgroup Hγ (●). The best-fit simulation was obtained using a distance of 4 Å and a D_{int} of 0.0005 nm^2/ms.

CH_2 and ω-CH_3 but quickly exceeds them and reaches a plateau by 150 ms, at which the experimental intensity is only ~50%. On the other hand, the 16 Å curve agrees with the experimental data at long mixing times but shows vanishing intensities for the first 50 ms, which contradicts the data. Thus, neither the short distance nor a long distance comparable to the monolayer thickness of POPC membranes describes the observed ω-CH_3 and CH_2 buildup curves well.

The 4 and 16 Å buildup curves were calculated using an interfacial diffusion coefficient (D_{int}) of 0.0025 nm^2/ms, a value optimized for colicin Ia channel domain in similar membranes (*35*). To better reproduce the experimental spin-diffusion behavior of CH_2 and ω-CH_3 at both short and long times, we reduced D_{int} to 0.0005 nm^2/ms. The resulting build-up curve for a 2 Å separation (solid line, Figure 7a) fits the measured CH_2 and ω-CH_3 spin diffusion well. The much smaller D_{int} may be explained by the larger mobility of PG-1 compared to that of the colicin Ia channel domain and by the lower ^1H densities of β-sheets compared to those of α-helices. Although this D_{int} is an adjustable parameter in the simulations, the different effects of the distance and the diffusion coefficient on the shape of the buildup curves indicate that the fitting is reasonable.

The spin-diffusion buildup curve for Hγ-to-peptide transfer (Figure 7b) exhibits a trend similar to that of the CH_2 and ω-CH_3 curves. A reasonable fit is obtained using a lipid−peptide separation of 4 Å and the same D_{int} of 0.0005 nm^2/ms. Combining all three spin-diffusion curves, we conclude that PG-1 contacts both the headgroup and the hydrophobic center of the POPC bilayer.

DISCUSSION

Peptide aggregation in lipid bilayers is important for understanding the mechanism of antimicrobial activity. For the β-sheet peptide PG-1, we have previously determined its orientation (*26*) and depth of insertion (*27*) in DLPC bilayers. The choice of the short chain DLPC was driven by the fact that these lipids maintain their macroscopic orientational order in the presence of high concentrations of PG-1 and that the peptide shows no sign of oligomerization, thus simplifying the studies. However, ultimately, we are interested in the more biologically relevant bilayer thickness of POPC. The current study compares the dynamic behavior of PG-1 in DLPC and POPC lipids and finds that PG-1 has a markedly reduced mobility in POPC membranes. The F12 ^{13}CO spectra in DLPC, DMPC, and POPC (Figure 1) indicate unambiguously that as the lipid chain length increases, so does the chemical shift anisotropy. In DLPC bilayers, the carbonyl carbons of both F12 and V16 have not only a significantly reduced δ but also a low η of ~0.1. Since F12 are V16 are located at the two ends of the β-hairpin (Figure 1) and self-rotation around the molecular axis is ruled out

by previous orientation measurements (*26*), the near-vanishing η can only result from uniaxial rotation of the peptide around the bilayer normal. In contrast, in POPC lipids, the carbonyl chemical shift tensor η increases to 0.87 for F12 and 0.79 for V16, while the order parameter increases to 0.79 for F12 and 0.69 for V16. These indicate that uniaxial rotation of PG-1 is inhibited in the thicker bilayer, and only internal segmental motions remain. The local segmental mobility differs between the two ends of the β-hairpin: the C-terminus (V16) is more flexible than the turn (F12), consistent with the solution NMR structure (*23*). Overall, the monotonic increase of δ from DLPC to DMPC and to POPC indicates that the inhibition of whole-body rotation of PG-1 is a consequence of the hydrophobic mismatch between the membrane thickness and the peptide length. We attribute this immobilization to peptide aggregation.

The low-temperature MAS spectra (Figure 3) confirm the motional narrowing of the chemical shift interaction of PG-1 in liquid-crystalline DLPC bilayers. The rigid-limit CSA values of V16 ^{13}CO are -77 and -82 ppm in DLPC and POPC bilayers, respectively. As expected, the low-temperature CSA tensor of the DLPC-bound PG-1 has an asymmetry parameter near 1, in dramatic contrast with the room-temperature value. Interestingly, the asymmetry parameter is somewhat smaller in POPC bilayers ($\eta = 0.72$) than in DLPC bilayers ($\eta = 0.80$) because of the downfield shift of the δ_{22} principal value by 3 ppm. According to quantum chemical calculations, an η value of 0.72 corresponds to an N$-$O distance of 2.7 Å while an η of 0.80 corresponds to an N$-$O distance of 3.0 Å. The dimer model of PG-1 indicates that the V16 C═O bond forms an intramolecular hydrogen bond with the L5 N$-$H group on the opposite strand; thus, it cannot accept intermolecular hydrogen bond donors. If this is true, then the 0.3 Å reduction in the hydrogen bond length for POPC-bound PG-1 could only result from aggregation-induced lateral compression of the β-strands such that the intramolecular hydrogen bond is shortened. Future ^{13}CO and ^{15}N labeling of V16 and L5 will permit a test of this hypothesis through distance measurements. Moreover, labeling of the C15 residue, which does participate in intermolecular hydrogen bonding in the dimer model, may provide direct information about PG-1 aggregation (*13*, *43*).

The near-rigid-limit C$\alpha-$Hα dipolar coupling of L5 in POPC bilayers at room temperature provides further support of PG-1 immobilization in long chain lipids. In comparison, the C$-$H coupling is reduced to 2 ± 1 kHz in DLPC bilayers, indicating large-amplitude motion. Since rotation around the β-strand axis and peptide wobbling can be ruled out, the only motion to scale down the C$-$H coupling is the rigid-body uniaxial rotation around the bilayer normal. Then the C$-$H order parameter corresponds to an angle of $118 \pm 4°$ between the L5 C$\alpha-$Hα bond and the DLPC membrane normal.

While the chemical shift and dipolar coupling spectra point to an absence of fast whole-body motions of PG-1 in POPC membranes, the CODEX experiment shows that slow reorientations do occur with a correlation time of 0.7 s. If aggregation is the sole source of immobilization, then one can calculate the volume of the PG-1 aggregate since the rotational diffusion rate is inversely proportional to the aggregate size. According to the two-dimensional hydrodynamic model (*18*), a cylindrical particle with a radius of a and a thickness of h has a rotational diffusion coefficient D_R of

$$D_R = \frac{1}{\tau_R} = \frac{k_B T}{4\pi\eta a^2 h}, \quad (2)$$

where τ_R is the rotational correlation time, η is the viscosity of the lipid bilayer, k_B is the Boltzmann constant, and T is the absolute temperature. If we assume that the PG-1 aggregate traverses the entire POPC bilayer, then h is $\sim$50 Å, phosphate to phosphate. A conservative upper-limit estimate of the membrane viscosity is 10 P (*44*). Using these values, a motional correlation time τ_R of 0.7 s yields a radius of 210 nm.

An aggregate radius of 210 nm is unrealistically large for the POPC/PG-1 mixture. Each PG-1 molecule has a van der Waals volume of $\sim$3 nm^3; thus, a domain size of 210 nm would correspond to tens of thousands of PG-1 molecules aggregated together. Such a large phase separation from the lipids would mean that only a small fraction of lipids are affected by the peptide. This contradicts the fact that the ^{31}P line shape of glass plate-aligned POPC lipids is significantly perturbed by PG-1 at *P*:*L* ratios above 1:30 (*26*). It is also inconsistent with the reduction of lipid ^{13}C T_2 relaxation times (*27*). Thus, we postulate that the hydrodynamic model is too simplistic for describing the motion of PG-1 in POPC membranes, and that aggregation is not the only cause of immobilization. Geometric constraints imposed by the lipid$-$peptide complexes may efficiently trap the peptide. The existence of such lipid$-$peptide complexes, possibly with a toroidal pore geometry, was suggested by the unusual and poorly oriented ^{31}P spectra of glass plate-aligned POPC/PG-1 membranes (*26*). Further contributing to the reduction of PG-1 motion may be electrostatic attractions between the anionic phospholipid headgroups and the cationic Arg side chains in the peptide.

The ^{1}H spin-diffusion experiments indicate that the immobilized PG-1 aggregates are in close contact with both the surface and the hydrophobic center of the bilayer. This location is consistent with a recent study of the insertion of PG-1 into phosphocholine monolayers at constant surface pressures (*45*). The proximity of PG-1 to the hydrophobic interior is also supported by the observation that the CH_2 and ω-CH_3 protons give very similar spin-diffusion buildup curves (Figure 7a). If PG-1 is surface-bound or only partially inserted, then one would expect a much slower buildup curve for the ω-CH_3 protons than for the CH_2 protons closer to the membrane surface. The conclusion that PG-1 aggregates reach the ends of the lipid chains is reasonable considering the possible size of the aggregate and the substantial hydrophobic patch in the central part of the β-hairpin. Moreover, in the context of the "toroidal pore" model (Figure 8), the PG-1 aggregates only need to span one monolayer because of the tight packing of the lipids that line the pore. This would still yield the observed spin-diffusion curves and would facilitate the snorkeling of the charged side chain of the Arg residues to the membrane$-$water interface (*46*).

The spin-diffusion results give the *average* separation between the peptide and the lipid segments. Since lipids have high dynamic disorder, the position of the individual segments along the bilayer normal has a sizable distribution. Non-negligible intermolecular contacts between the methyl

FIGURE 8: Model of PG-1 aggregation in POPC bilayers. PG-1 aggregates of varying sizes form complexes with the lipids to produce defects in the membrane. These oligomers contact both the surface and the hydrophobic interior of the membrane. The peptide aggregates do not undergo whole-body rotations on time scales shorter than 10^{-5} s but exhibit small-amplitude segmental motions at the N- and C-termini. The peptide also executes slow reorientations on the order of seconds.

group of the acyl chain and the headgroup of neighboring lipid molecules have been observed, indicating that the chain end methyl can occasionally bend back to the headgroup region of the bilayer (*47*). Therefore, the 4 Å separation between PG-1 and the lipid methyl groups should be interpreted in the context of the distributed nature of the lipid segmental positions (*48*). However, since the occasional bending back does not make the average depth of the methyl groups shorter than that of the CH_2 groups, the fact that the two gave similar spin-diffusion buildup curves strongly suggests that PG-1 spans most of the length of the hydrophobic chains.

It is worth noting that information about the location or insertion of PG-1 in POPC membranes cannot be inferred from oriented sample experiments since the POPC orientational order is destroyed by the peptide at concentrations necessary for the NMR experiments (*26*). It also cannot be obtained by comparing the paramagnetic relaxation enhancements of lipids and the peptide, since the dynamics of the peptide are fundamentally different from that of the lipids at room temperature (*27*). Thus, information obtained from the ^{1}H spin-diffusion experiment, while qualitative, provides a starting point for more precise characterization.

Figure 8 summarizes our current model of PG-1 immobilization and aggregation in POPC membranes. PG-1 forms oligomers of varying sizes that contact both the surface and the hydrophobic interior of the membrane. Although not yet directly observed, intermolecular hydrogen bonds are likely present in each aggregate. The peptide oligomers are immobilized on time scales shorter than 10^{-5} s except for segmental motions at the N- and C-termini, but do undergo slow rotational diffusion on the time scale of 1 s. Lipid molecules near the peptide adopt a distribution of orientations and complex with the peptide to create membrane defects that further restrict the peptide. These "boundary" lipids are more rigid than those far from the peptide.

ACKNOWLEDGMENT

We thank Prof. J. Kozak and Prof. X. Song for helpful discussions.

REFERENCES

1. Hancock, R. E., and Lehrer, R. (1998) *Trends Biotechnol. 16*, 82−88.
2. He, K., Ludtke, S. J., Worcester, D. L., and Huang, H. W. (1996) *Biophys. J. 70*, 2659−2666.
3. Duclohier, H., and Wroblewski, H. (2001) *J. Membr. Biol. 184*, 1−12.
4. Pouny, Y., Rapaport, D., Mor, A., Nicolas, P., and Shai, Y. (1992) *Biochemistry 31*, 12416−12423.
5. DeGrado, W. F., Gratkowski, H., and Lear, J. D. (2003) *Protein Sci. 12*, 647−665.
6. Gorman, P. M., Yip, C. M., Fraser, P. E., and Chakrabartty, A. (2003) *J. Mol. Biol. 325*, 743−757.
7. Nilsson, M. R., and Dobson, C. M. (2003) *Biochemistry 42*, 375−382.
8. Frost, D., Gorman, P. M., Yip, C. M., and Chakrabartty, A. (2003) *Eur. J. Biochem. 270*, 654−663.
9. Shai, Y. (1995) *Trends Biochem. Sci. 20*, 460−464.
10. Gazit, E., Burshtein, N., Ellar, D. J., Sawyer, T., and Shai, Y. (1997) *Biochemistry 36*, 15546−15554.
11. Eisenhawer, M., Cattarinussi, S., Kuhn, A., and Vogel, H. (2001) *Biochemistry 40*, 12321−12328.
12. Tycko, R. (2003) *Biochemistry 42*, 3151−3159.
13. Smith, S. O., Song, D., Shekar, S., Groesbeek, M., Ziliox, M., and Aimoto, S. (2001) *Biochemistry 40*, 6553−6558.
14. Fu, R., Cotten, M., and Cross, T. A. (2000) *J. Biomol. NMR 16*, 261−268.
15. Salgado, J., Grage, S. L., Kondejewski, L. H., Hodges, R. S., McElhaney, R. N., and Ulrich, A. S. (2001) *J. Biomol. NMR 21*, 191−208.
16. Yamaguchi, S., Huster, D., Waring, A., Lehrer, R. I., Kearney, W., Tack, B. F., and Hong, M. (2001) *Biophys. J. 81*, 2203−2214.
17. Nishimura, K., Kim, S., Zhang, L., and Cross, T. A. (2002) *Biochemistry 41*, 13170−13177.
18. Saffman, P. G., and Delbruck, M. (1975) *Proc. Natl. Acad. Sci. U.S.A. 72*, 3111−3113.
19. Kokryakov, V. N., Harwig, S. S., Panyutich, E. A., Shevchenko, A. A., Aleshina, G. M., Shamova, O. V., Korneva, H. A., and Lehrer, R. I. (1993) *FEBS Lett. 327*, 231−236.
20. Steinberg, D. A., Hurst, M. A., Fujii, C. A., Kung, A. H. C., Ho, J. F., Cheng, F. C., Loury, D. J., and Fiddes, J. C. (1997) *Antimicrob. Agents Chemother. 41*, 1738−1742.
21. Tamamura, H., Murakami, T., Horiuchi, S., Sugihara, K., Otaka, A., Takada, W., Ibuka, T., Waki, M., Yamamoto, N., and Fujii, N. (1995) *Chem. Pharm. Bull. 43*, 853−858.
22. Aumelas, A., Mangoni, M., Roumestand, C., Chiche, L., Despaux, E., Grassy, G., Calas, B., and Chavanieu, A. (1996) *Eur. J. Biochem. 237*, 575−583.
23. Fahrner, R. L., Dieckmann, T., Harwig, S. S., Lehrer, R. I., Eisenberg, D., and Feigon, J. (1996) *Chem. Biol. 3*, 543−550.
24. Roumestand, C., Louis, V., Aumelas, A., Grassy, G., Calas, B., and Chavanieu, A. (1998) *FEBS Lett. 421*, 263−267.
25. Yang, L., Weiss, T. M., Lehrer, R. I., and Huang, H. W. (2000) *Biophys. J. 79*, 2002−2009.
26. Yamaguchi, S., Waring, A., Hong, T., Lehrer, R., and Hong, M. (2002) *Biochemistry 41*, 9852−9862.
27. Buffy, J., Hong, T., Yamaguchi, S., Waring, A., Lehrer, R., and Hong, M. (2003) *Biophys. J. 85*, 2363−2373.
28. Herzfeld, J., and Berger, A. E. (1980) *J. Chem. Phys. 73*, 6021.
29. Bak, M., Rasmussen, T., and Nielsen, N. C. (2000) *J. Magn. Reson. 147*, 296−330.
30. Haeberlen, U. (1976) *High-Resolution NMR in Solids*: *Selective Averaging*, Academic Press, San Diego.
31. van Rossum, B. J., De Groot, C. P., Ladizhansky, V., Vega, S., and De Groot, H. J. M. (2000) *J. Am. Chem. Soc. 122*, 3465−3472.
32. Hong, M., Yao, X. L., Jakes, K., and Huster, D. (2002) *J. Phys. Chem. B 106*, 7355−7364.
33. de Azevedo, E. R., Bonagamba, T. J., Hu, W., and Schmidt-Rohr, K. (1999) *J. Am. Chem. Soc. 121*, 8411−8412.
34. Gullion, T., and Schaefer, J. (1989) *Adv. Magn. Reson. 13*, 57−83.
35. Huster, D., Yao, X. L., and Hong, M. (2002) *J. Am. Chem. Soc. 124*, 874−883.
36. Kumashiro, K. K., Schmidt-Rohr, K., Murphy, O. J., Ouellette, K. L., Cramer, W. A., and Thompson, L. K. (1998) *J. Am. Chem. Soc. 120*, 5043−5051.
37. Clauss, J., Schmidt-Rohr, K., and Spiess, H. W. (1993) *Acta Polym. 44*, 1−17.
38. Hartzell, C. J., Whitfeld, M., Oas, T. G., and Drobny, G. P. (1987) *J. Am. Chem. Soc. 109*, 5966−5969.

39. de Dios, A. C., and Oldfield, E. (1994) *J. Am. Chem. Soc. 116*, 11485−11488.
40. Wei, Y., Lee, D., and Ramamoorthy, A. (2001) *J. Am. Chem. Soc. 123*, 6118−6126.
41. Gu, Z., Zambrano, R., and McDermott, A. (1994) *J. Am. Chem. Soc. 116*, 6368−6372.
42. de Azevedo, E. R., Bonagamba, T. J., Hu, W., and Schmidt-Rohr, K. (2000) *J. Chem. Phys. 112*, 8988−9001.
43. Antzutkin, O. N., Balbach, J. J., Leapman, R. D., Rizzo, N. W., Reed, J., and Tycko, R. (2000) *Proc. Natl. Acad. Sci. U.S.A. 97*, 13045−13050.
44. Tamm, L. K. (1991) *Biochim. Biophys. Acta 1071*, 123−148.
45. Gidalevitz, D., Ishitsuka, Y., Muresan, A. S., Konovalov, O., Waring, A. J., Lehrer, R. I., and Lee, K. Y. (2003) *Proc. Natl. Acad. Sci. U.S.A. 100*, 6302−6307.
46. Segrest, J. P., De Loof, H., Dohlman, J. G., Brouillette, C. G., and Anantharamaiah, G. M. (1990) *Proteins 8*, 103−117.
47. Huster, D., Arnold, K., and Gawrisch, K. (1999) *J. Phys. Chem. 103*, 243−251.
48. White, S. H., and Wimley, W. C. (1999) *Annu. Rev. Biophys. Biomol. Struct. 28*, 319−365.

BI035187W